PHOTONICS Research

1.3 GHz E-O bandwidth GaN-based micro-LED for multi-gigabit visible light communication

Lei Wang,[1,†] Zixian Wei,[2,3,†] Chien-Ju Chen,[4,†] Lai Wang,[1,5] H. Y. Fu,[2,3,6] Li Zhang,[3] Kai-Chia Chen,[4] Meng-Chyi Wu,[4,7] Yuhan Dong,[3] Zhibiao Hao,[1] and Yi Luo[1]

[1]Beijing National Research Center for Information Science and Technology (BNRist), Department of Electronic Engineering, Tsinghua University, Beijing 100084, China
[2]Tsinghua-Berkeley Shenzhen Institute (TBSI), Tsinghua University, Shenzhen 518055, China
[3]Shenzhen International Graduate School, Tsinghua University, Shenzhen 518055, China
[4]Institute of Electronics Engineering, Taiwan Tsing Hua University, Hsinchu 30013, Taiwan, China
[5]e-mail: wanglai@tsinghua.edu.cn
[6]e-mail: hyfu@sz.tsinghua.edu.cn
[7]e-mail: mcwu@ee.nthu.edu.tw

Received 5 October 2020; revised 15 January 2021; accepted 2 February 2021; posted 2 February 2021 (Doc. ID 411863); published 29 April 2021

The data rate of a visible light communication (VLC) system is basically determined by the electrical-to-optical (E-O) bandwidth of its light-emitting diode (LED) source. In order to break through the intrinsic limitation of the carrier recombination rate on E-O bandwidth in conventional c-plane LEDs based on InGaN quantum wells, a blue micro-LED with an active region of nano-structured InGaN wetting layer is designed, fabricated, and packaged to realize a high-speed VLC system. The E-O bandwidth of the micro-LED can reach up to 1.3 GHz. Based on this high-speed micro-LED, we demonstrated a data rate of 2 Gbps with a bit error rate (BER) of 1.2×10^{-3} with simple on-off keying signal for a 3-m real-time VLC. In addition, a 4-Gbps VLC system using quadrature phase shift keying-orthogonal frequency-division multiplexing with a BER of 3.2×10^{-3} is also achieved for the same scenario. Among all the point-to-point VLC systems based on a single-pixel LED, this work has the highest distance-bandwidth product of 3 GHz·m and the highest distance-rate product of 12 Gbps·m.

https://doi.org/10.1364/PRJ.411863

1. INTRODUCTION

Visible light communication (VLC) is a promising solution for the next-generation high-speed access technology. As an important supplement to radio frequency (RF) communication, the available spectrum of VLC is over 3 orders of magnitude wider than the RF one. VLC can be combined with solid-state lighting, which has been widely implemented in many fields. In addition, VLC exhibits the advantages of low power consumption, no electromagnetic interference, eye-safety, and strong confidentiality [1]. It is simultaneously suitable for high-speed communication and illumination applications in special environments such as airports, hospitals, nuclear power plants, underwater [2], and deep space [3]. The electrical-to-optical (E-O) bandwidth of the light-emitting device is critical in a bandwidth-limited VLC system, although there are alternative approaches to optimize the responsivity and detectivity of photodetectors such as germanium/perovskite heterostructures and InGaN multiple quantum well (QW) micro-size photodetectors [4,5]. In comparison with commercial light-emitting diodes (LEDs), micro-size LEDs (micro-LEDs) based on III-nitride semiconductors with smaller active area and lower RC delay provide a promising approach to improve the E-O bandwidth [6,7]. Beneficial from the high E-O bandwidth, the micro-LED has great potential for high-speed VLC implementation [8,9]. The data rate of micro-LED-based VLC using non-return-to-zero on-off keying (NRZ-OOK) can reach up to 1 Gbps, and multi-Gbps data rates can be achieved by advanced modulation formats such as quadrature phase shift keying (QPSK), quadrature amplitude modulation (QAM), or orthogonal frequency-division multiplexing (OFDM) [10–17]. Tsonev *et al.* have demonstrated a VLC link with data rate over 3 Gbps based on a micro-LED using OFDM and then the data rate is extended to 5 Gbps afterwards [10–12]. Currently, single-pixel GaN-based micro-LEDs have been able to achieve a data rate of 10 Gbps by using bit-loading OFDM [13]. In addition, green-band, deep-ultraviolet, and perovskite materials have also been introduced for free-space communication applications [14–16]. Xie *et al.* adopted a series-structure

micro-LED array with 18-mW emitting power to realize a VLC system with a data rate of 5.18 Gbps [17].

However, traditional c-plane InGaN-based QW LED devices have long suffered from the limitation of the polarization-field-induced quantum-confined Stark effect (QCSE) [18]. The QCSE leads to a longer carrier lifetime in the QW at low current density, which limits the E-O bandwidth of devices. Therefore, high carrier concentration is required to screen the polarization field and shorten the carrier lifetime. A high E-O bandwidth of near 1 GHz has already been presented in micro-LEDs operating at a high current density [12,19]. However, the high current density will sacrifice the luminous efficiency of the LED which is well known as efficiency droop. Although there have been efforts to develop LED epitaxial structures optimized for shortening carrier lifetime under lower current density, the typical E-O bandwidth and operating current density of a c-plane micro-LED are still below 1 GHz and beyond 1 kA/cm^2, respectively. Achieving high E-O bandwidth LEDs under lower current density by growing InGaN-based QW devices on semi-polar or non-polar surfaces to suppress the QCSE is considered a fundamental solution [20–23]. For QW samples, the QCSE of semi-polar and non-polar samples will be significantly smaller than that of polar ones. High E-O bandwidth micro-LEDs beyond 1 GHz based on semi-polar and non-polar substrates have been demonstrated successfully [21,24]. Even though the injection current density for high E-O bandwidth of the semi-polar and non-polar micro-LEDs is significantly reduced, the high cost and small size of semi-polar and non-polar substrates limit the mass production of high-speed LEDs. In recent years, GaN-based quantum dots (QDs), as nanomaterials with extremely strong three-dimensional quantum confinement capabilities, have received tremendous attention and have been applied in various optoelectronic devices [25–30]. For QDs, the carrier lifetime can be efficiently decreased since the reduced dimensionality of the active region [31]. In addition, the strain can usually be relaxed during the QD formation process, so the QCSE will also be significantly smaller than that of the polar QW samples [32,33]. In traditional Stranski-Krastanov (SK) mode growth of InGaN QDs, an InGaN wetting layer is unavoidably formed beneath the QD layer [26]. However, light-emitting devices utilizing the InGaN wetting layer beneath the SK QDs are rarely reported. Here, we try to use the InGaN wetting layer as the active region of high-speed LEDs based on the traditional mature c-plane GaN growth and device fabrication process. Since the formation of the wetting layer is accompanied by the three-dimensional formation of QDs, the wetting layer also undergoes sufficient strain relaxation. Hence, the carrier lifetime in the wetting layer will be much shorter due to significantly suppressed QCSE, which is beneficial for the realization of high speed LEDs at lower current densities.

Figure 1 demonstrates a benchmark between our work and other groups, wherein our results are comparable with best results of the non-polar LEDs [21]. This can be concluded that we achieved the goal of high E-O bandwidth with low current density in traditional c-plane micro-LEDs. Furthermore, we will compare our E-O bandwidth of the wetting layer

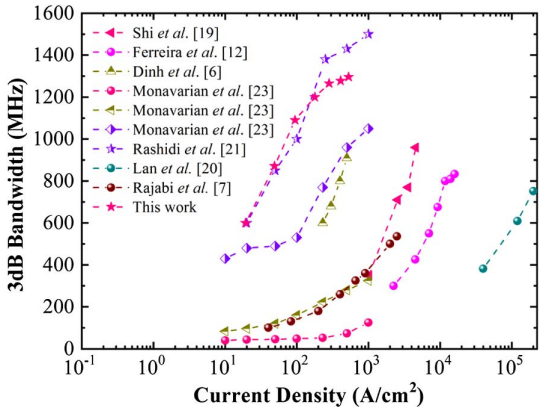

Fig. 1. E-O bandwidths versus current densities for the non-polar LED, semi-polar LED, and polar LED comparison between different reports.

micro-LED device with others. In terms of material growth, so far, almost all reported GaN-based high-speed LEDs are based on InGaN quantum well materials, including ones based on the traditional c-plane sapphire substrates and ones based on the non-polar/semi-polar GaN substrates. In this work, for the first time, self-assembly grown nano-structured InGaN wetting layers were adopted as the active layers of a high-speed LED and a 3-dB E-O bandwidth up to 1.3 GHz was achieved, which is tested on wafer after device fabrication. This result is much better than any other reports based on the c-plane epitaxy and is comparable to the best results based on the semi-polar/non-polar GaN substrates that have been reported, as shown in Fig. 1. However, considering the fact that non-polar/semi-polar materials-based LED devices must be grown on high-quality non-polar/semi-polar GaN homogeneous substrates, it has unavoidable disadvantages. First, such non-polar/semi-polar GaN substrates are so expensive that they are difficult to practically apply. Furthermore, the size of these substrates is difficult to enlarge (usually smaller than 1 cm^2), which directly leads to the difficulty of large-scale and low-cost commercial application. The InGaN wetting-layer-based high-speed micro-LEDs in our work are grown on traditional c-sapphire substrate, which is low in cost and large in size, and are fully compatible with current mature LED production processes, so our results are very beneficial to large-scale commercial applications. In addition, compared with the results of current densities as high as kA/cm^2 observed in other literature, our high-speed micro-LEDs realized a high E-O bandwidth of 1.3 GHz, while they only needed a current density of around 500 A/cm^2, as shown in Fig. 1. Excessive current density of the LED devices will significantly increase the power consumption, cause the droop effect, generate too much heat, and reduce the device lifetime.

In this paper, we present a 1-GHz modulation bandwidth VLC system based on a single-pixel micro-LED with an E-O bandwidth of 1.3 GHz under a current density of 528.5 A/cm^2. A 3-m VLC system with a 2-Gbps NRZ-OOK data rate with bit error rate (BER) of 1.2×10^{-3} and with 4-Gbps QPSK-OFDM with BER of 3.2×10^{-3} is

experimentally demonstrated and analyzed. To the authors' best knowledge, as for all the single-pixel LED-based point-to-point VLC systems, the present one achieved the highest distance-bandwidth product of 3 GHz·m and the highest distance-rate product of 12 Gbps·m using QPSK-OFDM. This work paves the way to next-generation illumination devices with InGaN nano-materials for high-speed VLC and shows great potential in actual free-space optical communication application.

2. MATERIALS, DEVICES, AND SYSTEM SETUP

A. Epitaxial Growth

The LED sample was grown on a 430-μm thick 2-in. (0001) sapphire substrate in an AIXTRON 2000HT metal-organic vapor phase epitaxy (MOVPE) system. The epitaxial structure of the sample is shown in Fig. 2(a), which contains a 1-μm undoped high-temperature GaN layer grown at 1040°C, a 3.5-μm Si-doped GaN layer grown with the same condition, an n-type 10-pairs of $In_{0.03}Ga_{0.97}N$ (3 nm)/GaN (3 nm) superlattices insertion layer grown at 740°C, a 1.5-nm InGaN wetting layer as the active region, a 20-nm undoped GaN barrier grown at 740°C, a 20-nm Mg-doped $Al_{0.2}Ga_{0.8}N$ electron blocking layer grown at 900°C, and a 150-nm Mg-doped GaN contact layer grown at 900°C. The InGaN wetting layer was grown at 655°C, employing a two-step growth interruption method, where an InGaN layer with a nominal thickness of 1.5 nm is grown, followed by a 20-s interruption of all the precursors, during which InGaN QDs as well as nano-structured wetting layer can be formed [34]. After the epitaxy, an annealing treatment at 550°C in an O_2 atmosphere outside the metal organic chemical vapor deposition (MOCVD) chamber was performed for 6 min to activate Mg dopants.

In order to observe the morphology of the QDs and wetting layer, another sample without capping layer was grown, which maintained the same structure beneath the active region. The surface morphology of the sample was measured by a Bruker Dimension Icon atomic force microscope (AFM).

A 10 μm × 10 μm AFM image of the sample is shown as Fig. 2(b). In previous work, green InGaN QDs with a density around 3×10^8–9×10^8 cm^{-2} can be grown by the two-step growth interruption method [26,34]. The nominal thickness of the InGaN film is usually 2–3 nm, and the growth temperature is between 640°C and 650°C. In this work, in order to reduce the density of QDs formed on the sample surface, the nominal thickness of the InGaN layer was reduced to 1.5 nm, and the growth temperature was also increased to 655°C to decompose the upper QDs as much as possible. The green ellipses in Fig. 2(b) indicate the remaining InGaN QDs on the sample surface, and the density of QDs is reduced to 2×10^7 cm^{-2}. Therefore, the wetting layer is distributed over most of the sample surface, and the luminescence of the sample is dominated by the wetting layer. Subsequent photoluminescence test also found that the peak wavelength of the sample is almost consistent with the wetting layer peak in the previous green QD samples [26].

In order to observe the morphology of the wetting layer sample in depth, a 1.5 μm × 1.5 μm AFM image is shown in Fig. 2(c). It can be seen that the nano-structured InGaN wetting layer appears like a broken nano-carpet. This unique nanostructure allows the wetting layer to fully release the compressive strain, thereby suppressing the QCSE and shortening the carrier life in the wetting layer. Figure 2(d) shows a

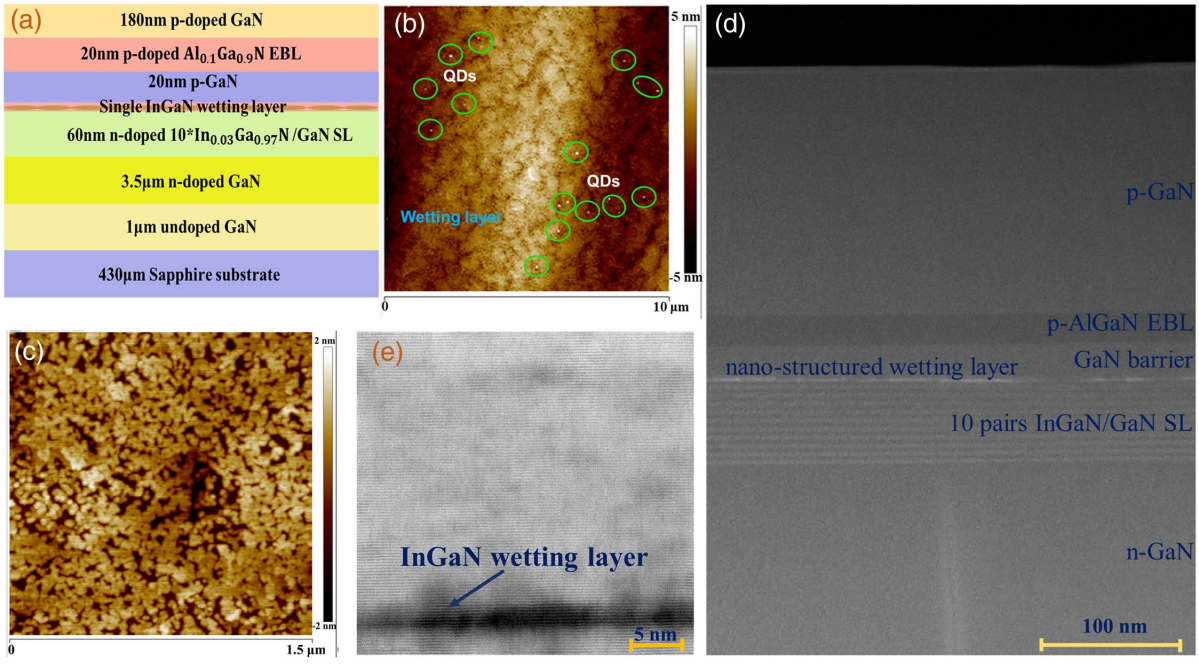

Fig. 2. (a) Schematic of the epitaxial structure of the wetting layer LED. (b) A 10 μm × 10 μm AFM image of the bare wetting layer sample. (c) A 1.5 μm × 1.5 μm AFM image of the nano-structured wetting layer. (d) A high-angle annular dark field scanning transmission electron microscope (HAADF STEM) image of the LED sample. (e) A magnified bright-field (BF) STEM image of the wetting layer region.

high-angle annular dark-field scanning transmission electron microscope (STEM) image of the LED sample, which demonstrates that the actual thickness of each layer of the sample is quite consistent with the design. A larger magnification bright-field STEM image shows that the wetting layer has a height around 2 nm, as shown in Fig. 2(e).

B. Structure, Fabrication, Optical and Electrical Characteristics of Micro-LED

In the fabrication process, we deposited a 700-nm indium tin oxide (ITO) layer on the micro-LED wafer since ITO would be the ohmic contact layer and the current spreading layer of the micro-LED. Next, the active region was defined by wet etching, which was then perfectly formed with a diameter of 75 μm. This is an optimal value, taking both electroluminescence (EL) intensity and E-O bandwidth into account. After defining the active region, we utilized dry etching by inductively coupled plasma-reactive etching to create the mesa of the micro-LED. A metal layer that works as a cathode is deposited on the exposed n-GaN. Because of the dry etching process, the mesa sidewall was then passivated by the SiO_2 layer mainly for lowering leakage current through sidewall defect. Eventually, a ring-shaped electrode was deposited onto the ITO ohmic layer, which can decrease the light blocking effect for the emissive light of the micro-LED. The device 3D structure schematic diagram is illustrated in Fig. 3(a). Figure 3(b) shows the image of the top view of the mesa/p-pad (75 μm/100 μm in diameter) for the LED observed by SEM (JSM-7000F). We adopt transistor-outline window-can (TO-CAN) with short gold thread as the packaged format which avoids bandwidth loss by introducing as little parasitic capacitance as possible.

This part mainly conducts the optical and electrical characteristics measurement of the nano-structured wetting layer micro-LED chip on wafer before packaging and Fig. 4(a) presents the L–J–V characteristics of the device testing on wafer. The threshold voltage is roughly equal to 3.5 V corresponding to the emitting optical power of 0.4 mW, and the maximum output optical power is ∼1.12 mW. The external quantum efficiency (EQE) measurement results are shown in Fig. 4(b), in which the maximum EQE reaches 2.5% at 22.6 A/cm^2 and the efficiency decreases to 0.8% at 1132 A/cm^2. The relatively low EQE of 2.5% depends on both light extraction efficiency (LEE) and carrier injection efficiency. For the former, as a flat sapphire substrate rather than a patterned sapphire substrate was used for epitaxy, the LEE is

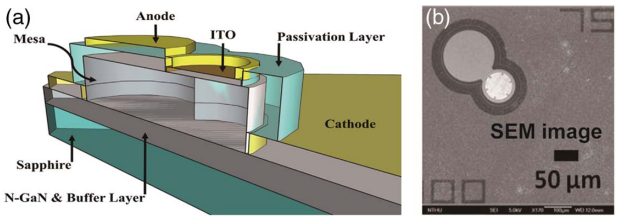

Fig. 3. (a) 3D view of the designed cross-sectional structure for the micro-LED. (b) The image of the top view of the mesa/anode (75 μm/100 μm in diameter) for the micro-LED observed by scanning electron microscopy (SEM, JSM-7000F).

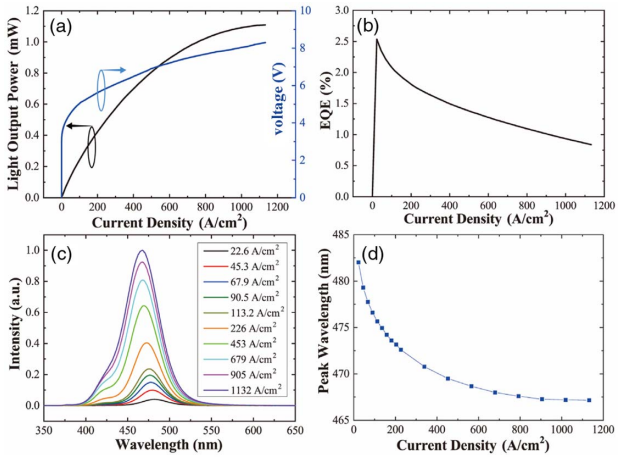

Fig. 4. (a) Light-current density-voltage (L–J–V) characteristics for the micro-LED and the EQE measurement of the samples. (b) The external quantum efficiency versus applied current densities. (c) The emissive spectra of the micro-LED. (d) The value of peak wavelength shifts with different current densities.

extremely low due to total reflection. If the patterned sapphire substrates or other roughening methods are used, the LEE can be further improved. As for the latter, carrier overflow without being captured by the active region occurs as only a single wetting layer is adopted. As the injection current of 20 mA is reached, the corresponding voltage is defined as the forwarding voltage (V_F). From the curve, V_F equals 6.7 V, which is caused by the non-optimal epitaxial and chip process conditions. Figure 4(c) shows the EL spectra as a function of the current density from 22.6 to 1132 A/cm^2 (1 to 50 mA), which have also been measured for encapsulated LEDs by using an integrating sphere. The peak around 410–420 nm can be attributed to the emission from the leakage carriers in the p-GaN. As the current density increases from 0 to 1 kA/cm^2, the emission wavelength of the micro-LED is blueshifted from 481 to 467 nm, and the blueshift amount is about 14 nm, as shown in Fig. 4(d). The blueshift amount is comparable to the reported non-polar blue high-speed LEDs, implying it is induced by the band-filling effect rather than polarization screening and the QCSE has been suppressed in the wetting layer [21].

C. VLC System Setup

Figure 5 shows the experimental schematic of the micro-LED-based VLC system with 3-m link. Then, Fig. 6(a) shows the experimental setup photography of the micro-LED-based VLC system with 3-m communication distance in a typical indoor environment. Figures 6(b) and 6(c) represent the micro-LED transmitter and the avalanche photodiode (APD) receiver, respectively. For the NRZ-OOK real-time communication, an integration bit error rate tester (BERT, MP2100A, Anritsu) integrating pulse pattern generator (PPG), error detector, and sampling oscilloscope is used for measuring eye diagrams and BERs at different data rates with NRZ-OOK modulation format. The PPG of the BERT generates a $2^{31}-1$ bits digital baseband pseudo-random-binary-signal with 0.8 V peak-to-peak voltage which further passes through a wide-bandwidth

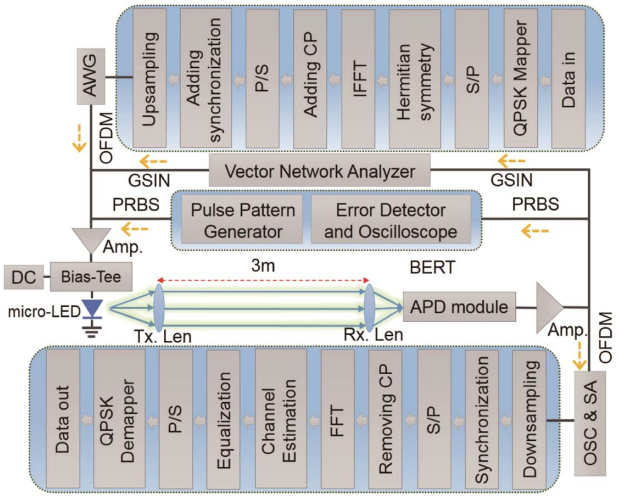

Fig. 5. Schematic of the micro-LED-based VLC system in a typical indoor environment over 3-m link.

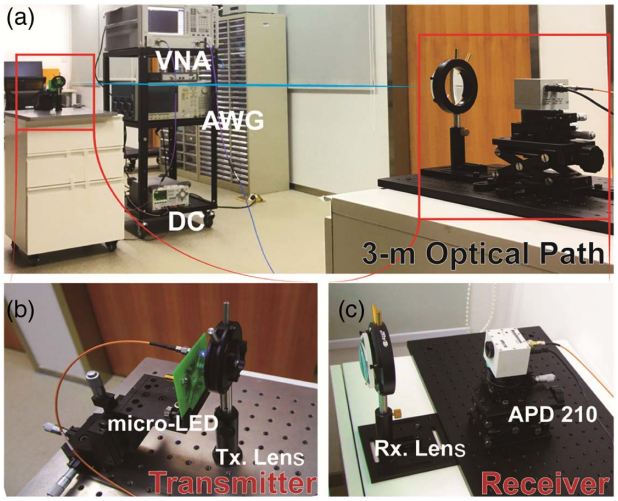

Fig. 6. (a) Photograph of the micro-LED-based VLC system in a typical indoor environment. (b) Wetting layer micro-LED-based transmitter and (c) APD module-based receiver.

amplifier (ZX60-43+, 0.5 to 4000 MHz, Mini-circuit) and is then input into the RF port of the bias-tee (ZFBT-6GW+, 0.1 to 6000 MHz, Mini-circuit). A power supply (DP832, Rigol) provides direct current (DC) and then the superimposed RF + DC signal combined by the bias-tee directly drives the packaged micro-LED to emit a modulated continuous light signal. A frog eye lens put in front of the micro-LED is used to improve the directivity of the weak light signal. After 3-m transmission, the optical signal is focused on the sensitive area of the APD module by using a 50-mm focal length convex lens. The high-sensitivity APD module with a bandwidth of 1 GHz (APD210, Menlo Systems) receives the optical signal and converts it into an electric signal which is amplified through an extra amplifier (ZX60-43+, Mini-circuit). The recovered digital baseband signal is then fed into a digital sampling oscilloscope module and the error detector in BERT so that the eye diagram can be captured and the BER can be tested at different data rates. A vector network analyzer (N5227A, Agilent) connecting the transmitter and the receiver is used to obtain the modulation bandwidth of the entire VLC system, as shown in Fig. 6(a).

The QPSK-OFDM experimental demonstration can be divided into real-time communication and off-line processing. The signal is modulated and demodulated off-line, as shown in Fig. 5. First, the NRZ-OOK data stream is generated and mapped into the QPSK-OFDM signal format with 256 carriers via a MATLAB program. The modulated serial signal is converted into parallel and then Hermitian symmetry is imposed before performing an inverse fast Fourier transform. The cyclic prefix (CP) of 1/16 is inserted into the low-speed parallel blocks which are then converted back into a serial format. In addition, in order to obtain a suitable format for demodulation, a synchronization sequence is added in front of the frame, which is then uploaded into an arbitrary waveform generator (AWG, AWG7000A, Tektronix). The AWG generates an up-sampled RF signal to conduct the real-time communication experiments. At the receiver, a high-speed sampling oscilloscope (DPO75902SX, Tektronix) is used for recording the down-sampled signal with different data rates under various injection current densities. Meanwhile, a signal analyzer (N9030B, Keysight) is used to observe the signal spectrum. Recorded data have been further processed in MATLAB. After synchronization, the high-speed serial data stream is converted into low-speed parallel data blocks and the CP has been removed. Parallel time-domain signals are transformed into frequency-domain signals by a fast Fourier transform. After further performing equalization through channel estimation, the serial QAM signal is de-mapped into a baseband signal that has been then compared with the original input signal to evaluate the BER.

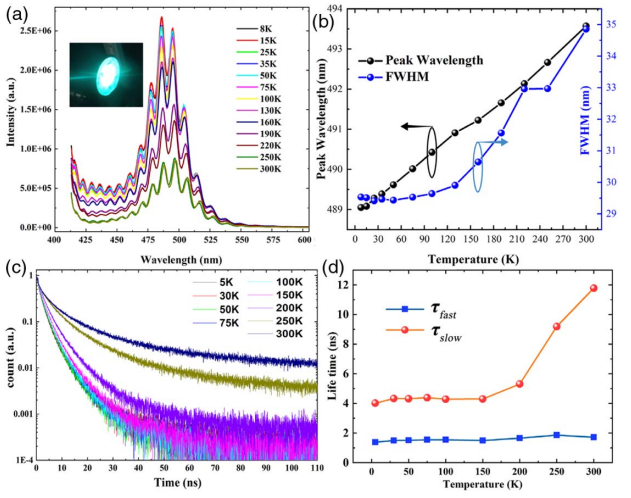

Fig. 7. (a) TDPL spectra of the sample. The inset is a photograph of the sample excited by the laser. (b) The temperature dependence of peak wavelength and FWHM. (c) TRPL measurement. (d) Calculated τ_{fast} and τ_{slow} of the decay curves at different temperatures using a bi-exponential decay model.

3. RESULTS AND DISCUSSION

A. Optical Properties and Carrier Dynamics

Detailed optical property characterization of the LED sample is performed by temperature-dependent photoluminescence (TDPL) measurement, as shown in Figs. 7(a) and 7(b). As shown in Fig. 7(a), the emission wavelength is around 490 nm and the equally spaced fluctuations on the spectrum are due to the Fabry–Perot interference between the smooth sample surface and the sapphire–GaN interface. The temperature dependence of the peak wavelength and the full width at half-maximum (FWHM) is presented in Fig. 7(b), where FWHM is defined as the width of the spectrum at half the maximum intensity. The PL spectra are measured in a cryogenic chamber, which can be cooled down to 8 K by a closed cycle liquid helium compressor. A Coherent 405-nm laser with a power density of 4 W/cm^2 is used as the excitation source. The sample glows cyan, roughly around 490 nm, and as the temperature increases from 8 to 300 K, the peak wavelength is redshifted by 4.5 nm, while the FWHM is slightly reduced first, followed by an increase of 5.5 nm.

Temperature-dependent time-resolved photoluminescence (TRPL) measurement is carried out to reveal the carrier dynamics of the LED sample, and the detection wavelength is set according to the emission peak. The TRPL is performed using a tunable femtosecond laser with a 380-nm excitation wavelength and 100-fs FWHM pulse width. The repetition rate and average energy of each pulse are recorded to be 8 MHz and 62.5 pJ, respectively. Figure 7(c) shows the temperature-dependent TRPL results, which show that as the temperature increases, the carrier lifetime of the sample does not change much at first, but when the temperature exceeds 150 K the carrier lifetime begins to increase. Furthermore, TRPL curves can be fitted using a bi-exponential decay model, which is defined as follows:

$$I = A_1 e^{-t/\tau_{\text{fast}}} + A_2 e^{-t/\tau_{\text{slow}}}, \tag{1}$$

where I represents the intensity, t represents time, τ is the carrier recombination lifetime, and τ_{fast} and τ_{slow} refer to the fast decay lifetime and the slow decay lifetime in the TRPL curve, respectively. Figure 7(d) shows τ_{fast} and τ_{slow} at different temperatures. According to the results, as the temperature increases from 5 to 300 K, τ_{fast} is always maintained at around 1.4 ns, while τ_{slow} stays at 4 ns at first, but after 150 K it quickly increases to 11.7 ns. Carrier lifetime is a key parameter for VLC devices. When it is small enough, it signifies that carriers can quickly recombine, meaning that the modulation speed of the devices can also increase. Compared to the conventional QW devices with a τ as long as several nanoseconds, which limits the device E-O bandwidth to the order of megahertz, the τ as short as 1 ns of the sample demonstrates a great potential for gigahertz-range VLC.

B. E-O Bandwidth of Micro-LED Measured on Wafer

High-speed LEDs based on polar InGaN QWs generally need to inject a current density as high as 10 kA/cm^2 to suppress the QCSE in the device through Coulomb screening [14], in order to achieve high modulation bandwidth. Our device can achieve a modulation bandwidth up to 1.1 GHz at a very low current density of 95 A/cm^2, which is comparable to the best reported non-polar result [21]. From Fig. 8(a), we can observe that the 3-dB E-O bandwidth of the micro-LED increases with increasing of the driving current density and equals 1.3 GHz at the current density of 528.5 A/cm^2. Figure 8(b) is the normalized frequency response versus frequency at various current densities.

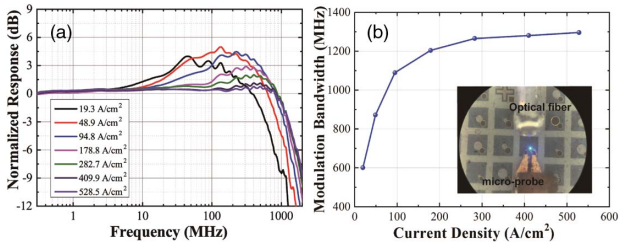

Fig. 8. (a) E-O bandwidth of the wetting layer micro-LED on wafer measurement for different current densities. (b) Original normalized frequency response. Inset: the device under RF GS microprobe was observed by optical microscope.

In our work, the following bandwidth measurements are strictly distinguished in different situations, which include the E-O bandwidth of the micro-LED device tested on wafer, the E-O bandwidth of the packaged micro-LED device, and the modulation bandwidth of the VLC system. Obviously, considering the actual application, the values of bandwidth will decrease from the micro-LED chip to the packaged micro-LED device, and then decrease from the packaged micro-LED device to the modulation bandwidth of the VLC system. Therefore, the back-to-back data transmission can obtain maximum data rate over an optical fiber. For real experimental demonstration of the VLC system, the data rate is lower than back-to-back limited by communication distance, packaging of devices, optical power, channel loss, and other factors.

The abovementioned E-O bandwidth value of 1.3 GHz for c-plane polar micro-LEDs before packaging is tested on wafer using a plastic optical fiber to export light which exhibits the LED under a radio-frequency ground-signal (RF GS) microprobe. It is not difficult to notice that there is no communication distance in some publications, which is impossible in the real application of VLC systems [23]. Therefore, the data rate from testing on wafer by the GS micro-probe with collecting by plastic optical fiber over 0 m free-space communication distance as shown in Fig. 8(b) is totally different from a real system compared with the micro-LED-based VLC system in Fig. 6(a). The measured modulation bandwidth of 1 GHz is limited by the bandwidth of the APD receiver and influenced by the free-space channel conditions and the attenuation of the optical power, which results in the decline of bandwidth from 1.3 to 1 GHz.

C. System Communication Performances Measurement

The normalized frequency response of the micro-LED-based VLC system with a 3-m link is shown in Fig. 9(a), which illustrates the modulation bandwidth characteristics under various current densities. Figure 9(b) depicts the 3-dB modulation bandwidth of the VLC system extracted from Fig. 9(a) in which

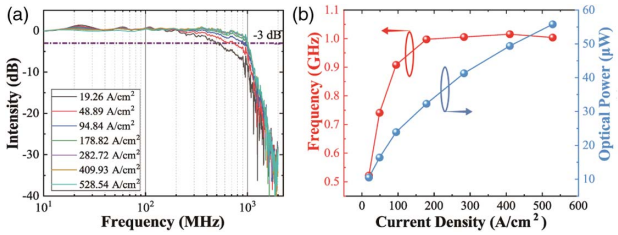

Fig. 9. (a) Normalized frequency responses of the VLC system with various current densities. (b) The extracted 3-dB modulation bandwidth and received optical power.

the curve tends to rise sharply and stabilize at around 1 GHz with the increase of the current density. Without any hardware equalization technique, it can reach 998 MHz at a current density as low as 178.82 A/cm^2 and 1 GHz at a current density of 528.54 A/cm^2, indicating that the micro-LED packaging performs well. However, the modulation bandwidth is slightly decreased at a current density of 528.54 A/cm^2, which can be further explained by the influence of modulation depth characteristics. In this work, the E-O bandwidth of the micro-LED device is strictly distinguished from the modulation bandwidth of the VLC system, which decreased from 1.3 to 1 GHz mainly by the bandwidth limit of the 1-GHz APD module. This limitation will be resolved when a higher-bandwidth APD is used. In addition, because of its low-sensitivity characteristics, the positive-intrinsic-negative (PIN) photodiode cannot reconstruct the original signal from the weak receiving power emitted from the micro-LED after 3-m transmission distance. Figure 10 gives the optical power comparison between the transmitter side and the receiver side, and the optical difference can be obtained under specific driving voltage. The red line marks the current density versus voltage ($L-I$) curve of the packaged 75-μm micro-LED. Under the premise of well adjusting the optical path through the dual lens, the attenuation can be reduced very low, which means that a longer communication distance can also be realized over the free-space link.

The communication performance of the micro-LED-based VLC system using the NRZ-OOK modulation format is evaluated under various data rates. The BER values as a function of

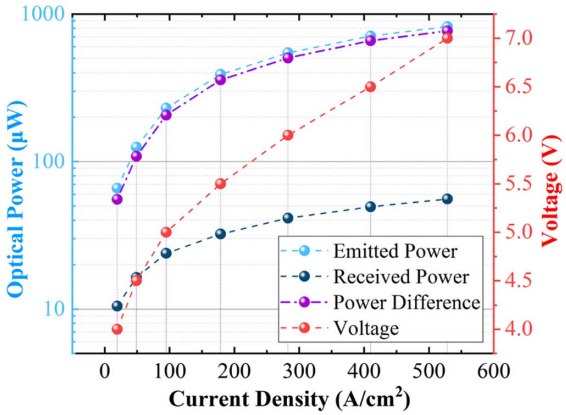

Fig. 10. Comparison of optical power between the emitter side and the receiver side and the $I-V$ properties of the micro-LED.

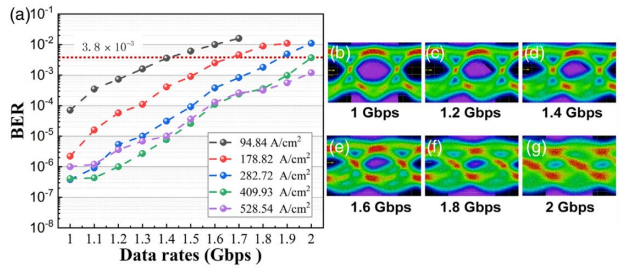

Fig. 11. (a) Data rates versus BER for the experimentally obtained results and the eye diagrams of (b) 1.0 Gbps, (c) 1.2 Gbps, (d) 1.4 Gbps, (e) 1.6 Gbps, (f) 1.8 Gbps, and (g) 2.0 Gbps data rates at the driving current density of 528.54 A/cm^2.

data rates for the entire system are shown in Fig. 11. When the data rate is lower than 1 Gbps, error-free VLC can be achieved. It can be observed that as the micro-LED current density increases from 94.8 to 528.54 A/cm^2, the BER is visibly improved. When the driving current densities are 94.84 A/cm^2, 178.82 A/cm^2, and 282.72 A/cm^2, the data rates that can be achieved are 1.4 Gbps, 1.6 Gbps, and 1.8 Gbps with corresponding BERs of 3.6×10^{-3}, 2.5×10^{-3}, and 1.8×10^{-3}, respectively. However, at the same modulation depth of 0.8 V, if the current density further increases, the BER performance will deteriorate as the linear range of the micro-LED will be exceeded. At the current density of 409.93 A/cm^2, the BER value changes from 4.1×10^{-7} to 3.7×10^{-3} with the data rate increasing from 1 to 2 Gbps. At the current density of 528.54 A/cm^2, instead, the BER value equals 1.0×10^{-6} at 1 Gbps data rate and 1.2×10^{-3} at 2 Gbps data rate. With a BER below the forward error correction (FEC) threshold of 3.8×10^{-3}, the highest data rate of this VLC can reach tops at 2 Gbps when the current density is kept at 409.93 A/cm^2 and at 528.54 A/cm^2. To the best of our knowledge, this is the highest data rate in a real-time NRZ-OOK VLC point-to-point link using a single-pixel LED without any equalization technique. The right figures show the eye diagrams of 1.0 Gbps, 1.2 Gbps, 1.4 Gbps,

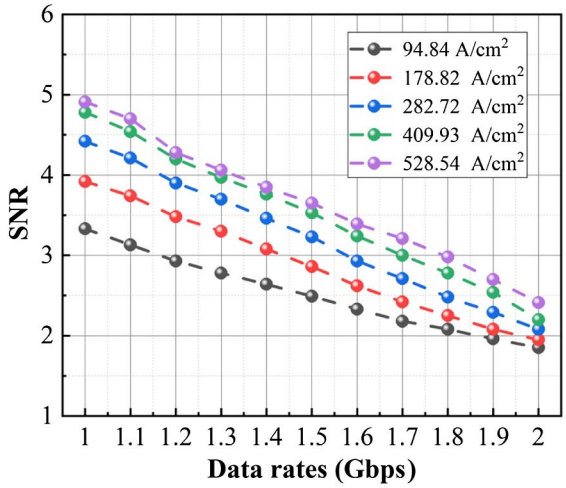

Fig. 12. SNR versus data rate of the micro-LED-based VLC system using NRZ-OOK format at different current densities.

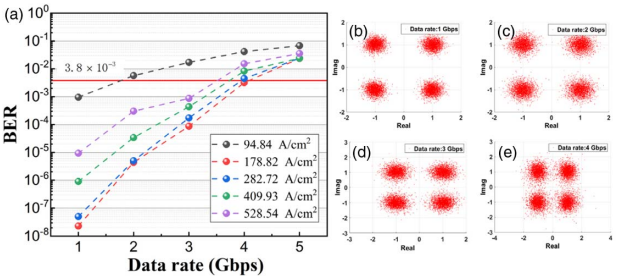

Fig. 13. (a) Data rate and related BER of QPSK-OFDM at different current densities and the constellation diagrams with the data rate change of (b) 1 Gbps, (c) 2 Gbps, (d) 3 Gbps, and (e) 4 Gbps at the current density of 528.54 A/cm^2.

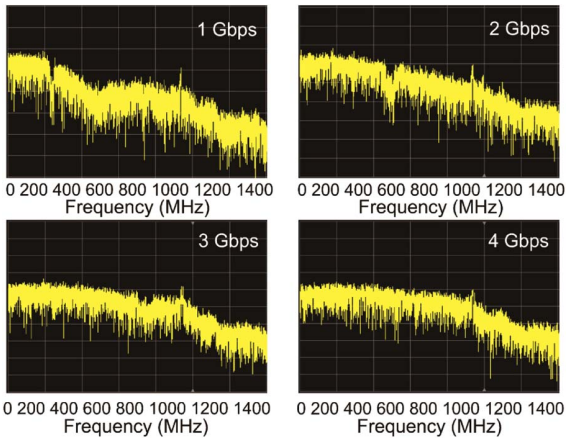

Fig. 14. Corresponding frequency spectrograms with the data rate change from 1 to 4 Gbps at the current density of 178.82 A/cm^2.

1.6 Gbps, 1.8 Gbps, and 2.0 Gbps all at 528.54 A/cm^2 current density, respectively. A wide-open eye diagram can be captured indicating a low BER when the data rate varies from 1 to 1.4 Gbps. The aperture of the eye diagram visibly decreases, and it is almost null at 2.0 Gbps corresponding to the BER of 1.2×10^{-3}.

In Fig. 12, the SNR of the micro-LED-based VLC system versus data rate at various driving current densities over the 3-m transmission link was measured. It has then been used to evaluate communication performances in terms of BER and eye diagrams under the NRZ-OOK modulation format. Low DC current density will result in a smaller SNR, as shown from the vertical comparison of different driving current densities at the same data rate, which is consistent with the tendency observed in Ref. [13]. On the other hand, the SNR will slightly worsen with the increase of the data rate. The SNR variation from 1 to 2 Gbps varies at different driving current densities, and becomes more evident at the higher current densities. When the current density equals 94.8 A/cm^2, the SNR equals 3.33 and 1.85 at the data rates of 1 Gbps and 2 Gbps, respectively. At the current density of 528.54 A/cm^2, the SNR decreases from 4.91 to 2.41 for the same change in data rate. It is worth mentioning that we have not increased the driving current density at 528 A/cm^2 of the micro-LED in the high-speed characterization. However, the initial *L–J–V* curves and spectral characterization go up to 1132 A/cm^2 which are measured on chip before packaging. TO-CAN packaging of the micro-LED and the length of the measurement time jointly result in the difference of thermal dissipation of the devices. Limited by the peak-to-peak voltage of the input signal from the BERT, the SNR is lower than the SNR of the QPSK-OFDM signal in the experiment.

For demonstrating further high-speed VLC using the high-order modulation format, we used an AWG to generate QPSK-OFDM signals at different rates and stored the signals with a sampling oscilloscope. Figure 13 shows the various data rates versus BER at different driving current densities. Compared with the NRZ-OOK signal, the highest data rate of 4.0 Gbps with the BER of 3.2×10^{-3} occurs at a current density of 178.82 A/cm^2 due to the linearity regime of the micro-LED, signal peak to average power ratio, and responsibility of the APD. At the current density of 94.84 A/cm^2, the maximum data rate of the VLC system only reaches 1.0 Gbps with the BER of 9.6×10^{-4}. As for the current densities from 282.72 A/cm^2 to 528.54 A/cm^2, the maximum data rates are all 3 Gbps with the BER of 1.7×10^{-4}, 4.3×10^{-4}, and 8.7×10^{-4}, respectively. Figure 13 also shows four constellation diagrams of QPSK-OFDM signals with the data rates ranging from 1.0 to 4.0 Gbps at a current density of 178.82 A/cm^2. The modulation bandwidth of the VLC system is around 1 GHz, allowing 256 subcarriers for OFDM modulation without redistributing their energy. The BER worsens significantly when the data rate is 5 Gbps. The corresponding frequency spectrograms of the QPSK-OFDM signal at the receiver side from data rates of 1–4 Gbps are shown in Fig. 14. The QPSK-OFDM signal with 1 GHz bandwidth and 256 subcarriers is used to achieve a data rate of 4 Gbps with a BER of 3.2×10^{-3} within the FEC threshold. The corresponding performance indicators of the wetting layer micro-LED-based VLC system using NRZ-OOK and QPSK-OFDM are shown in Table 1.

Table 1. Experimental Performance of Wetting Layer Micro-LED-Based VLC System with Various Modulation Formats at Distance of 3 m

Current Density (A/cm^2)	Highest Data Rate of NRZ-OOK (Gbps)	BER of NRZ-OOK	Highest Data Rate of QPSK-OFDM (Gbps)	BER of QPSK-OFDM
94.84	1.4	3.6×10^{-3}	1.0	9.6×10^{-4}
178.82	1.6	2.5×10^{-3}	4.0	3.2×10^{-3}
282.72	1.8	1.8×10^{-3}	3.0	1.7×10^{-4}
409.93	2.0	3.7×10^{-3}	3.0	4.3×10^{-4}
528.54	2.0	1.2×10^{-3}	3.0	8.7×10^{-4}

Table 2. Performance of VLC Systems Based on Single-Pixeled Micro-LED (Summary of Part of Existing Works)

Year	Group	μLED[a] Type	Optical Power (mW)	Bandwidth (MHz)	Modulation Format	Highest Data Rate (Gbps)	BER	Distance (m)
2014	[10] D. Tsonev *et al.*	Blue μLED	4.5	60	mQAM-OFDM[b]	3	<0.002	0.05
2015	[11] J. McKendry *et al.*	UV[c] μLED	2.5	130	mQAM-OFDM	3.32	2.1×10^{-3}	–
2016	[12] R. Ferreira *et al.*	Blue μLED	2.7	800	NRZ-OOK[d]	1.7	<FEC	0.5
			5.7		PAM4[e]	3.5		0.75
					mQAM-OFDM	5		0.75
2017	[13] M. Islim *et al.*	Violet μLED	~0.32	655	mQAM-OFDM	7.91	<FEC	~0.26
2017	[35] X. Liu *et al.*	μLED	0.8	~230	NRZ-OOK	1.3	3.4×10^{-3}	3
						1	3.2×10^{-3}	10
						0.87	3.5×10^{-3}	16
2018	[16] S. Mei *et al.*	μLED + YQDs[f]	16 lux	85	NRZ-OOK	0.3	2×10^{-3}	
2018	[36] X. Liu *et al.*	μLED-based detector	–	–	NRZ-OOK	0.185	3.5×10^{-3}	~1
2019	[17] E. Xie *et al.*	3 × 3 μLED arrays	~18	285	NRZ-OOK	2.1	<FEC	0.3
					PAM4	2.55		0.3
					mQAM-OFDM	5.18		0.3
2019	[15] X. He *et al.*	UV μLEDs	0.196	438	NRZ-OOK	0.8	3.8×10^{-3}	0.3
					mQAM-OFDM	1.1		
2019	[37] J. Carreira *et al.*	Dual-color μLED arrays	0.85/1.04	427/134	mQAM-OFDM	3.35	–	0.3
2020	Our work	Blue wetting layer μLED	0.82[g]	1000	NRZ-OOK	2	<FEC	3
					QPSK-OFDM[h]	4		3

[a]μLED: micro-size LED.
[b]QAM-OFDM: quadrature amplitude modulation-orthogonal frequency division multiplexing.
[c]UV: ultraviolet.
[d]NRZ-OOK: non-return-to-zero on-off-keying.
[e]PAM4: pulse-amplitude-modulation 4-level.
[f]YQDs: yellow quantum dots.
[g]The emitting optical power at the current density of 528.54 A/cm^2 after packaging as shown in Fig. 10.
[h]QPSK-OFDM: quadrature phase shift keying-orthogonal frequency-division multiplexing.

Finally, we compare our wetting layer micro-LED-based VLC system with other point-to-point VLC systems based on single-pixeled LEDs which have been reported in other literature. As shown in Table 2, compared with the works of Islim *et al.* with a distance-rate product of 2.0566 Gbps · m and the works of Xie *et al.* with a distance-rate product of 1.554 Gbps · m [13,17], combining with communication distance over 3 m, our micro-LED based VLC system has obvious performance advantages including the highest distance-bandwidth product of 3 GHz·m and the highest distance-rate product of 12 Gbps·m based on the QPSK-OFDM format, and all these records can only be obtained by taking advantage of the superior performance of our micro-LED device.

4. CONCLUSION

In conclusion, for solving the intrinsic bandwidth limitation of luminescent devices in the VLC systems, self-assembly grown nano-structured InGaN wetting layers were adopted as the active layers of a high-speed LED. A 480-nm blue micro-LED with 1.3 GHz E-O bandwidth on c-plane GaN is presented in this paper which is much higher than any other reports based on the c-plane epitaxy. The VLC system modulation bandwidth can reach 1 GHz after using the packaged micro-LED as transmitter. In addition, to give a comprehensive evaluation, we employed the micro-LEDs in a VLC system and demonstrate a 3-m data transmission over air channel, which has the highest distance-bandwidth product of 3 GHz·m among all the point-to-point VLC systems based on a single-pixel LED. By employing a $2^{31}-1$ bits NRZ-OOK signal without using non-linearity mitigation or equalization techniques, the received eye diagrams are clear when observed at 2 Gbps data rates with a low current density of 407 A/cm^2 and a BER of 1.2×10^{-3}. We achieved a record-breaking data rate among all the single-pixel LED-based point-to-point VLC systems using simple NRZ-OOK modulation. As for QPSK-OFDM, we demonstrated a data rate of 4 Gbps with a BER of 3.2×10^{-3}, which is the highest distance-rate product of 12 Gbps·m among all the point-to-point single-pixel LED-based VLC systems. It further proves the promising potential of our proposed InGaN wetting layer micro-LED in the next generation of high-speed VLC.

Funding. National Key Research and Development Program of China (2016YFB0401803); National Natural Science Foundation of China (61822404, 61974080); Shenzhen Science and Technology Innovation Commission (JCYJ20180507183815699); Tsinghua-Berkeley Shenzhen Institute (TBSI) Faculty Start-up Fund; Shenzhen Fundamental Research Project (JCYJ20170817161720819); Overseas Research Cooperation Fund of Tsinghua Shenzhen International Graduate School (HW2018003).

Disclosures. The authors declare no conflicts of interest.

†These authors contributed equally to this paper.

REFERENCES

1. A. Tsiatmas, C. P. M. J. Baggen, F. M. J. Willems, J. M. G. Linnartz, and J. W. M. Bergmans, "An illumination perspective on visible light communications," IEEE Commun. Mag. **52**, 64–71 (2014).
2. Z. Zeng, S. Fu, H. Zhang, Y. Dong, and J. Cheng, "A survey of underwater optical wireless communications," IEEE Commun. Surveys Tuts. **19**, 204–238 (2017).
3. C. Tsai, C. Cheng, H. Kuo, and G. Lin, "Toward high-speed visible laser lighting based optical wireless communications," Prog. Quantum Electron. **67**, 100225 (2019).
4. W. Hu, H. Cong, W. Huang, Y. Huang, L. Chen, A. Pan, and C. Xue, "Germanium/perovskite heterostructure for high-performance and broadband photodetector from visible to infrared telecommunication band," Light Sci. Appl. **8**, 106 (2019).
5. K. Ho, R. Chen, G. Liu, C. Shen, J. Holguin-Lerma, A. A. Al-Saggaf, T. K. Ng, M. Alouini, J. He, and B. S. Ooi, "3.2 gigabit-per-second visible light communication link with InGaN/GaN MQW micro-photodetector," Opt. Express **26**, 3037–3045 (2018).
6. D. V. Dinh, Z. Quan, B. Roycroft, P. J. Parbrook, and B. Corbett, "GHz bandwidth semipolar (112-2) InGaN/GaN light-emitting diodes," Opt. Lett. **41**, 5752–5755 (2016).
7. K. Rajabi, J. Wang, J. Jin, Y. Xing, L. Wang, Y. Han, C. Sun, Z. Hao, Y. Luo, K. Qian, C. Chen, and M. Wu, "Improving modulation bandwidth of c-plane GaN-based light-emitting diodes by an ultra-thin quantum wells design," Opt. Express **26**, 24985–24991 (2018).
8. H. Han, H. Lin, C. Lin, W. Chong, J. Li, K. Chen, P. Yu, T. Chen, H. Chen, K. Lau, and H. Kuo, "Resonant-enhanced full-color emission of quantum-dot-based micro LED display technology," Opt. Express **23**, 32504–32515 (2015).
9. T. Wu, C. Sher, Y. Lin, C. Lee, S. Liang, Y. Lu, S. H. Chen, W. Guo, H. Kuo, and Z. Chen, "Mini-LED and micro-LED: promising candidates for the next generation display technology," Appl. Sci. **8**, 1557 (2018).
10. D. Tsonev, H. Chun, S. Rajbhandari, J. J. D. McKendry, S. Videv, E. Gu, M. Haji, S. Watson, A. E. Kelly, G. Faulkner, M. D. Dawson, H. Haas, and D. O'Brien, "A 3-Gb/s single-LED OFDM-based wireless VLC link using a gallium nitride μLED," IEEE Photonics Technol. Lett. **26**, 637–640 (2014).
11. J. J. D. McKendry, D. Tsonev, R. Ferreira, S. Videv, A. D. Griffiths, S. Watson, E. Gu, A. E. Kelly, H. Haas, and M. D. Dawson, "Gb/s single-LED OFDM-based VLC using violet and UV gallium nitride μLEDs," in *IEEE Summer Topicals Meeting Series (SUM)* (2015), pp. 175–176.
12. R. X. G. Ferreira, E. Xie, J. J. D. McKendry, S. Rajbhandari, H. Chun, G. Faulkner, S. Watson, A. E. Kelly, E. Gu, R. V. Penty, I. H. White, D. C. O. Brien, and M. D. Dawson, "High bandwidth GaN-based micro-LEDs for multi-Gb/s visible light communications," IEEE Photonics Technol. Lett. **28**, 2023–2026 (2016).
13. M. S. Islim, R. X. Ferreira, X. He, E. Xie, S. Videv, S. Viola, S. Watson, N. Bamiedakis, R. V. Penty, I. H. White, A. E. Kelly, E. Gu, H. Haas, and M. D. Dawson, "Towards 10 Gb/s orthogonal frequency division multiplexing-based visible light communication using a GaN violet micro-LED," Photon. Res. **5**, A35–A43 (2017).
14. C. Chen, J. Yan, D. Chen, K. Lin, K. Feng, and M. Wu, "A 520-nm green GaN LED with high bandwidth and low current density for gigabits OFDM data communication," in *Optical Fiber Communication Conference (OFC)* (2018), paper Th2A.18.
15. X. He, E. Xie, M. S. Islim, A. A. Purwita, J. J. D. McKendry, E. Gu, H. Haas, and M. D. Dawson, "1 Gbps free-space deep-ultraviolet communications based on III-nitride micro-LEDs emitting at 262 nm," Photon. Res. **7**, B41–B47 (2019).
16. S. Mei, X. Liu, W. Zhang, R. Liu, L. Zheng, R. Guo, and P. Tian, "High-bandwidth white-light system combining a micro-LED with perovskite quantum dots for visible light communication," ACS Appl. Mater. Interface **10**, 5641–5648 (2018).
17. E. Xie, X. He, M. S. Islim, A. A. Purwita, J. J. D. McKendry, E. Gu, H. Haas, and M. D. Dawson, "High-speed visible light communication based on a III-nitride series-biased micro-LED array," J. Lightwave Technol. **37**, 1180–1186 (2019).
18. S. Tsai, C. Lu, and C. Liu, "Piezoelectric effect on compensation of the quantum-confined Stark effect in InGaN/GaN multiple quantum wells based green light-emitting diodes," Nano Energy **28**, 373–379 (2016).
19. J. Shi, K. Chi, J. Wun, J. E. Bowers, Y. Shih, and J. Sheu, "III-nitride-based cyan light-emitting diodes with GHz bandwidth for high-speed visible light communication," IEEE Electron Device Lett. **37**, 894–897 (2016).
20. H. Lan, I. Tseng, H. Kao, Y. Lin, G. Lin, and C. Wu, "752-MHz modulation bandwidth of high-speed blue micro light-emitting diodes," IEEE J. Quantum Electron. **54**, 3300106 (2018).
21. A. Rashidi, M. Monavarian, A. Aragon, A. Rishinaramangalam, and D. Feezell, "Nonpolar m-plane InGaN/GaN micro-scale light-emitting diode with 1.5 GHz modulation bandwidth," IEEE Electron Device Lett. **39**, 520–523 (2018).
22. M. Monavarian, A. Rashidi, A. A. Aragon, M. Nami, S. H. Oh, S. P. DenBaars, and D. Feezell, "Trade-off between bandwidth and efficiency in semipolar (2021) InGaN/GaN single-and multiple-quantum-well light-emitting diodes," Appl. Phys. Lett. **112**, 191102 (2018).
23. M. Monavarian, A. Rashidi, A. A. Aragon, S. H. Oh, A. K. Rishinaramangalam, S. P. DenBaars, and D. Feezell, "Impact of crystal orientation on the modulation bandwidth of InGaN/GaN light-emitting diodes," Appl. Phys. Lett. **112**, 041104 (2018).
24. M. Haemmer, B. Roycroft, M. Akhter, D. V. Dinh, Z. Quan, J. Zhao, P. J. Parbrook, and B. Corbett, "Size-dependent bandwidth of semipolar (1122) light-emitting-diodes," IEEE Photonics Technol. Lett. **30**, 439–442 (2018).
25. H. Gao, F. Yan, Y. Zhang, J. Li, Y. Zeng, and J. Wang, "Growth of nonpolar a-plane GaN on nano-patterned r-plane sapphire substrates," Appl. Surf. Sci. **255**, 3664–3668 (2009).
26. L. Wang, L. Wang, J. Yu, Z. Hao, Y. Luo, C. Sun, Y. Han, B. Xiong, J. Wang, and H. Li, "Abnormal Stranski–Krastanov mode growth of green InGaN quantum dots: morphology, optical properties, and applications in light-emitting devices," ACS Appl. Mater. Interface **11**, 1228–1238 (2019).
27. A. Hu, H. Tian, Q. Liu, L. Wang, L. Wang, X. He, Y. Luo, and X. Guo, "Graphene on self-assembled InGaN quantum dots enabling ultrahighly sensitive photodetectors," Adv. Opt. Mater. **7**, 1801792 (2019).
28. M. Arita, F. Le Roux, M. J. Holmes, S. Kako, and Y. Arakawa, "Ultraclean single photon emission from a GaN quantum dot," Nano Lett. **17**, 2902–2907 (2017).
29. Z. Gačević, M. Holmes, E. Chernysheva, M. Müller, A. Torres-Pardo, P. Veit, F. Bertram, J. Christen, J. M. González Calbet, Y. Arakawa, E. Calleja, and S. Lazić, "Emission of linearly polarized single photons from quantum dots contained in nonpolar, semipolar, and polar sections of pencil-like InGaN/GaN nanowires," ACS Photonics **4**, 657–664 (2017).
30. D. Wang, T. Zhu, R. A. Oliver, and E. L. Hu, "Ultra-low-threshold InGaN/GaN quantum dot micro-ring lasers," Opt. Lett. **43**, 799–802 (2018).
31. G. Weng, Y. Mei, J. Liu, W. Hofmann, L. Ying, J. Zhang, Y. Bu, Z. Li, H. Yang, and B. Zhang, "Low threshold continuous-wave lasing of yellow-green InGaN-QD vertical-cavity surface-emitting lasers," Opt. Express **24**, 15546–15553 (2016).
32. E. P. O. Reilly and S. Schulz, "Theory of reduced built-in polarization field in nitride-based quantum dots," Phys. Rev. B **82**, 033411 (2010).
33. M. Zhang, P. Bhattacharya, and W. Guo, "InGaN/GaN self-organized quantum dot green light emitting diodes with reduced efficiency droop," Appl. Phys. Lett. **97**, 011103 (2010).
34. L. Wang, D. Yang, Z. Hao, and Y. Luo, "Metal–organic–vapor phase epitaxy of InGaN quantum dots and their applications in light-emitting diodes," Chin. Phys. B **24**, 067303 (2015).
35. X. Liu, P. Tian, Z. Wei, S. Yi, Y. Huang, X. Zhou, Z.-J. Qiu, L. Hu, Z. Fang, C. Cong, L. Zheng, and R. Liu, "Gbps long-distance real-time visible light communications using a high-bandwidth GaN-based micro-LED," IEEE Photonics J. **9**, 7204909 (2017).

36. X. Liu, R. Lin, Z. Qian, H. Chen, X. Zhou, G. Zhou, X. Cui, X. Zhou, L. Zheng, R. Liu, and P. Tian, "An InGaN micro-LED based photodetector array for high-speed parallel visible light communication," in *Asia Communications and Photonics Conference (ACP)* (2018), pp. 1–3.

37. J. F. C. Carreira, E. Xie, R. Bian, C. Chen, J. J. D. McKendry, B. Guilhabert, H. Haas, E. Gu, and M. D. Dawson, "On-chip GaN-based dual-color micro-LED arrays and their application in visible light communication," Opt. Express **27**, A1517–A1528 (2019).